
VOLUME 114
ISSUE 5
17 MAY 2010
ELSEVIER
Remote Sensing of Environment
http://www.elsevier.com/locate/rse

Remote Sensing of Environment 114 (2010) 1026–1037

Contents lists available at ScienceDirect

Remote Sensing of Environment

journal homepage: www.elsevier.com/locate/rse

Influence of forest cover fraction on L-band soil moisture retrievals from heterogeneous pixels using multi-angular observations

J.P. Grant [a,b,*], A.A. Van de Griend [a], J.-P. Wigneron [b], K. Saleh [c], R. Panciera [d], J.P. Walker [d]

[a] Department of Hydrology and Geo-environmental Sciences, Vrije Universiteit Amsterdam, De Boelelaan 1085, 1081 HV, Amsterdam, The Netherlands
[b] Institut National de la Recherche Agronomique (INRA) - EPHYSE, Bordeaux, France
[c] Geography Department, University of Cambridge, United Kingdom
[d] Department of Civil and Environmental Engineering, University of Melbourne, Australia

ARTICLE INFO

Article history:
Received 1 June 2009
Received in revised form 18 December 2009
Accepted 20 December 2009

Keywords:
Passive microwaves
Forest
Soil moisture
Heterogeneity

ABSTRACT

Airborne L-band data from the Australian National Airborne Field Experiment 2005 (NAFE '05) field campaign were used to investigate the influence of fractional forest cover on soil moisture retrievals from heterogeneous (grass/forest) pixels. This study is, to our knowledge, the first to use experimental data on this subject and was done in view of the SMOS mission, in order to contribute to calibration/validation studies and the analysis of heterogeneous surfaces. Because the multi-angle observations were contained in swaths, swaths were used instead of pixels as the basic surface unit in this study. Simultaneous retrievals of soil moisture (*SM*) and vegetation optical depth (τ_{NAD}) were undertaken by inversion of the L-MEB zero-order radiative transfer model. This was done for two different retrieval configurations, the first consisting of swath-effective values of *SM* and τ_{NAD} and the second consisting of values of *SM* and τ_{NAD} for the non-forested (i.e. grass) fraction of the swath, with forest emission known from forward modelling. Model inputs for non-retrieved parameters were either default values taken from the literature or site- and time-specific values obtained from observations of nearby homogeneous swaths gathered during the same flight. The main focus of this study was on retrieval behaviour for various soil moisture conditions and forest fractions. Area-averaged retrieval results were generally very reasonable for both retrieval configurations. When retrieving swath-effective values of *SM* and τ_{NAD}, τ_{NAD} showed an increased overestimation with increased forest fraction. Highest retrieved values of *SM* were found at intermediate values of forest fraction. The results show the difficulty in flagging upper limits of pixel forest fraction during soil moisture retrievals, besides the fact that erroneous parameter values can lead to high errors in retrieved *SM*, especially in wet conditions. This study is the first to give a realistic idea of the errors and uncertainties involved in soil moisture retrievals from partly forested swaths, and as such will contribute to a better understanding of SMOS calibration/validation issues.

1. Introduction

ESA's Soil Moisture and Ocean Salinity (SMOS) mission, launched in November 2009, carries a multi-angle interferometric L-band (1.4 GHz) radiometer for monitoring soil moisture and ocean salinity at global scale (Kerr et al., 2001). Spatial resolution of the instrument is around 40 km at nadir view, which means that most pixels of the earth's surface will be heterogeneous, consisting of a mixture of forest, crops, grass and bare soil. The target error for SMOS is below 0.04 m^3m^{-3} volumetric soil moisture. Studies involving soil moisture retrievals over crops and grassland have indicated that this target error can be achieved (e.g. Pardé et al., 2004; Wigneron et al., 2007; Saleh et al., 2007). However, soil moisture retrievals over forested areas are expected to give poorer results, due to the higher attenuating effect of the denser vegetation cover. Previously, soil moisture retrievals over homogeneous forested areas using experimental observations at L-band have been attempted in several small-scale studies (e.g. Chauhan et al., 1999; Lang et al., 2001; Lang et al., 2006). The results of these studies showed some sensitivity to soil moisture, depending on forest biomass and ground conditions. However, Lang et al. (2001) indicated the need for accurate measurement of ground temperature in order to achieve these results. A modelling study by Della Vecchia, Saleh, et al. (2006) also found an appreciable sensitivity to soil moisture over forests. Although temperate deciduous and coniferous forests have been found to have a reasonably high transmissivity, ranging from 0.4–0.6 (Grant et al., 2008; Guglielmetti et al., 2008; Guglielmetti et al., 2007;

* Corresponding author. Department of Hydrology and Geo-environmental Sciences, Vrije Universiteit Amsterdam, De Boelelaan 1085, 1081 HV, Amsterdam, The Netherlands.
E-mail address: jennifer.grant@falw.vu.nl (J.P. Grant).

0034-4257/$ – see front matter
doi:10.1016/j.rse.2009.12.016

Della Vecchia, Ferrazzoli, et al., 2006; Hallikainen et al., 2000), above-canopy L-band observations can show only a small sensitivity to changes in soil moisture content due to the obscuring effect of the litter and understory layers, if these are present (e.g. Grant et al., 2007 and 2009). A relatively invariable forest emission could actually be an asset in soil moisture retrievals over heterogeneous pixels containing forest, as the soil moisture of the non-forested part of the pixel might still be retrieved with the required accuracy if the emission of the forested part of the pixel is modelled correctly. The current study investigates these issues for heterogeneous pixels containing a mix of grassland and open Eucalypt forest. This type of forest has not been previously studied and differs from the temperate forests mentioned above due to (among other things) its open character and low litter cover.

To date, all known studies concerning soil moisture retrievals from heterogeneous forest pixels have been based on model simulations (Van de Griend et al., 2003; Van de Griend et al., 2004; Loew, 2008), rather than experimental data. The first two of these studies concluded that ignoring the *a priori* knowledge of the forest cover fraction α results in large errors in soil moisture retrieval if $\alpha \geq 10\%$, but if α is known and $\leq 50\%$, soil moisture in the non-forested area can be determined with a precision better than the 0.04 m^3m^{-3} target error for SMOS. The third study found a similar result, but again stressed the importance of knowing the surface temperature to within 4 K. That study also indicated that soil moisture retrievals over mixed forest pixels can show a good temporal evolution of soil moisture although the retrieval results themselves are biased. Retrieval accuracy was also found to depend on scale, increasing with decreasing spatial resolution until levelling out above a 10 km resolution.

While the above modelling studies present rather optimistic results, the studies are restricted to a limited range of moisture and land cover conditions, and, importantly, the results have not been verified with experimental data. Moreover, significant assumptions are made concerning parameter values. Especially, forest optical depth was assumed to be much higher than values found from recent field experiments (1–1.5 compared to 0.4–0.6).

In view of the SMOS mission, the current study seeks to validate the results of previous modelling studies using large-scale experimental data which include both homogeneous and heterogeneous pixels, different land cover fractions, and different soil moisture conditions. The National Airborne Field Experiment 2005 (NAFE '05) field campaign (Panciera et al., 2008) is well suited to this task. The main objective of the current study is thus to better understand and quantify the influence of forested areas on the soil moisture retrieval from heterogeneous pixels.

2. Materials

2.1. Site description

The area of study (lat/lon (32° 8′ 42″ S, 150° 6′ 43.1994″ E) to (32° 11′ 6″ S, 150° 9′ 7.1994″ E)) covered part of the 'Roscommon' farm. This area was part of the larger 'Krui' study area covering the Krui River subcatchment, which lies within the Goulburn River catchment in southeast Australia. The location of Roscommon within the catchment is outlined in (Panciera et al., 2008), while Fig. 1 shows the farm boundaries, forest areas and flight lines in more detail.

The study area has an average elevation of 300 masl and is characterised by native grassland and relatively open Eucalypt forest areas. The forested surfaces were generally found on the more steep and rocky parts of the landscape (gently rolling with elevation differences up to ~15 m), whereas the flatter parts had been cleared for grazing.

The grassland areas consisted of native grass spp., with an average vegetation height estimated to be ~30 cm. Average grass Normalized Difference Vegetation Index (NDVI) during the experiment was 0.60. This was calculated using a handheld Model 100BX Radiometer with 4 channels (450–520, 520–600, 630–690 and 760–900 nm). NDVI readings were taken at sixteen 50 m spaced locations across a 150 m by 150 m area (the so-called 'high resolution area', cf. Panciera et al., 2008). At each location, three readings were taken of each spectral band. Estimates of leaf area index (LAI) derived from MODIS data at 250 m resolution were around 1.8 m^2m^{-2} for the entire campaign. Grass water content was estimated to be around 0.5 ± 0.2 kg based on destructive measurements of the weight difference between wet and dry biomass.

The forest areas consisted mainly of Box (*Eucalyptus* spp.), Ironbark (*Eucalyptus* spp.) and some Black Cypress-pine (*Callitris endlicheri*). Fish-eye photographs were taken of the Eucalypt vegetation, from which the fraction cover was determined to be ~39% and the LAI was estimated at 2.5. MODIS images showed that forest LAI did not noticeably change during the experiment. The understory was an open-heath formation consisting mainly of Sifton bush (*Cassinia quinquefaria*). Some litter was present on the ground and formed a generally very thin (~ 0.5 cm) layer. Litter dry bulk density was 0.15 ± 0.05 gcm^{-3}. It is estimated that around 10–15% of the forest floor consisted of bed rock, with the remainder covered by sandy soil (67% sand, 15% clay) with a bulk density of 1.22 g cm^{-3} and a porosity of 0.437. Field observations found the thickness of the soil layer to be highly variable, however, more detailed information on this parameter is unavailable.

2.2. Data

The airborne L-band measurements used in the current study were made using the dual-polarised Polarimetric L-band Multibeam Radiometer (PLMR) on 1st, 8th, 10th, 15th, and 22nd November 2005. Rather heavy precipitation occurred at the very beginning of the experiment, followed by a long drying-up period and finally some scattered rainfall at the end of the experiment. Precipitation data recorded at the Stanley station (approx. 8 km northwest of Roscommon) were available from the Goulburn River experimental data set (Rüdiger et al., 2007). Table 1 shows an overview of meteorological conditions over the study area on the relevant flight days and times.

PLMR observations were made in a pushbroom configuration at four different altitudes; however, the current study used only the lowest (approximately 190 m above ground level) altitude data in order to obtain a sufficient number of swaths. At this altitude the nominal ground resolution (−3 dB footprint) was 62.5 m at nadir. Observations were made every second at incidence angles of +/−7°, +/−21.5° and +/−38.5°, with the six footprints covering a total swath of approximately 375 m. Observations where the aircraft pitch/roll angle was >5° were filtered out. More detailed information on PLMR and the flight characteristics can be found in (Panciera et al., 2008).

Thermal infrared temperatures T_{IR} were obtained with a FLIR ThermaCam S60 thermal imager (spectral range 7.5–13 μm), which was also on board the aircraft carrying PLMR. The FLIR had a ~1 m resolution at the lowest altitude flight and obtained T_{IR} using an overall scene emissivity of 0.98, which is a value often used for vegetation in the thermal infrared range. One FLIR image covered approximately the same area as the PLMR swath. For each PLMR swath, only minimum, maximum and average T_{IR} values for the whole swath were used.

A Landsat 5 TM image from October 2005 (spatial resolution 25 m) was used to define seven land cover types (dense forest, open woodland, native grass, bare soil/low LAI, crops, cloud and cloud shadow), based on a combination of supervised and unsupervised classification methods. In the current study, the 'dense forest' and 'open woodland' classes were joined together to define forest areas, while the 'native grass' class was used to define the grassland areas (cf. Fig. 1).

Ground measurements of the top 5 cm soil moisture content were taken using a portable Stevens Water Hydraprobe® sensor. A site-specific calibration of this sensor against gravimetric samples in the field and laboratory has indicated that the data are accurate to within

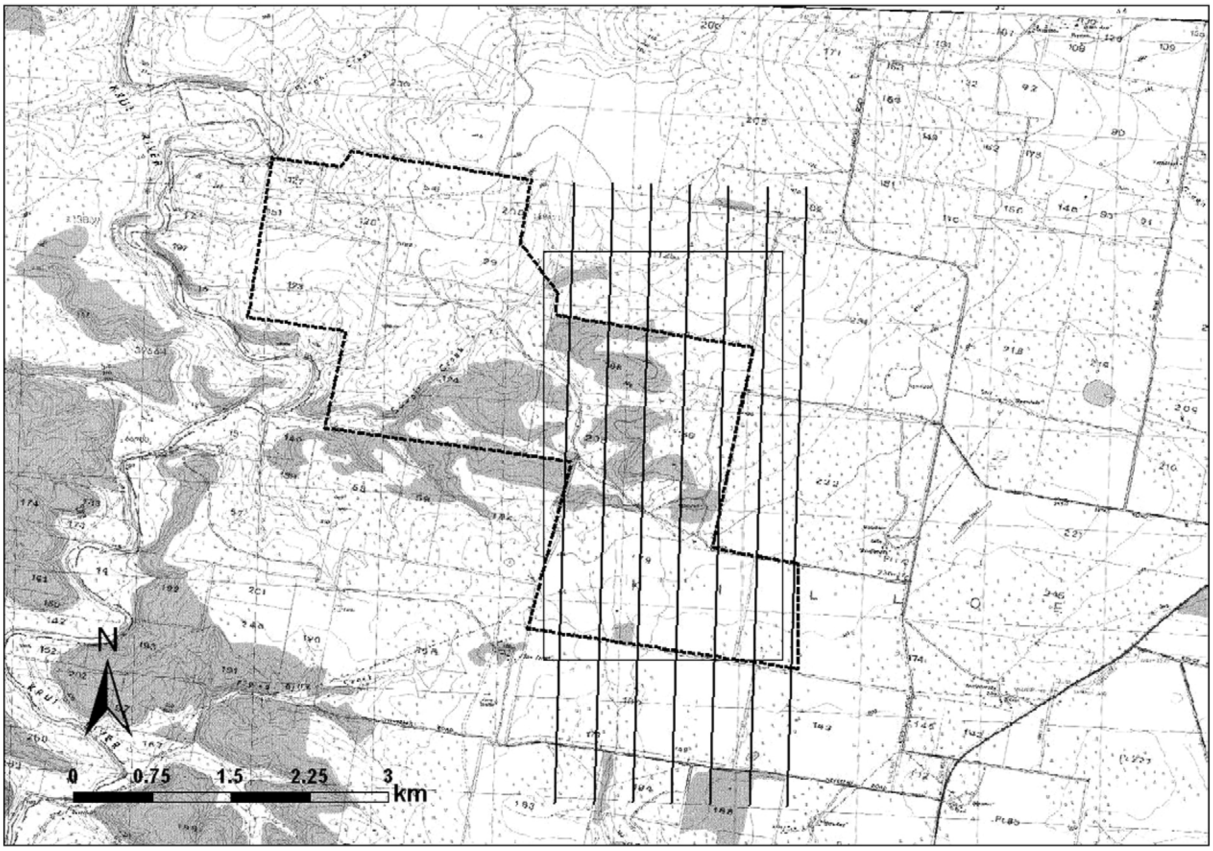

Fig. 1. Topographic map of the area around Roscommon farm. The farm boundary is given by the dotted line, the thick solid lines show the seven PLMR flight lines at approximately 150 m altitude above ground level and the thin-lined rectangle indicates the approximate study area. The forest areas are coloured in grey.

$\pm 0.033\ m^3 m^{-3}$ (Merlin et al., 2007). Approximately 10–15 measurements were taken at random throughout the forest area per day and approximately 60–100 throughout the grassland areas, although these were concentrated in the south-west part of the farm. These measurements were part of the 'farm-scale' sampling (cf. Panciera et al., 2008) done at Roscommon. All available data points within the current study area (Section 2.1) were taken into account, irrespective of the resolution grid they belonged to.

Finally, field measurements of temperature were made at two fixed locations on Roscommon farm: one in a grassland area and one in the forest. Soil temperatures at the grassland location were obtained at 1 cm depth with Unidata 6507A/10 sensor, and (for 22nd Nov. only) at 2.5 cm depth with a T107 sensor, every 20 min. At the fixed forest location, temperatures were obtained every 10 min from thermocouples installed at 2 cm depth in the soil, on the soil surface, 2 cm within the tree trunk at breast height, and at 5 m and 7.5 m in the canopy.

3. Methods

3.1. L-MEB

The radiative transfer model used was the L-band Microwave Emission of the Biosphere (L-MEB) model (Wigneron et al., 2007), which forms the base of the SMOS Level 2 Soil Moisture Algorithm. The main L-MEB equation for a vegetation-covered soil is based on a simplified zero-order radiative transfer approach of the 'τ-ω' type (Kirdyashev et al., 1979; Mo et al., 1982), as shown in Eq. (1):

$$T_B^{P,\theta} = T_S \cdot \left(1-R_{S,corr}^{P,\theta}\right) \cdot \gamma^{P,\theta} + \left(1-\omega^P\right) \cdot \left(1-\gamma^{P,\theta}\right) \cdot T_C \cdot \left(1 + R_{S,corr}^{P,\theta} \cdot \gamma^{P,\theta}\right) + R_{S,corr}^{P,\theta} \cdot T_{B,sky} \cdot \left(\gamma^{P,\theta}\right)^2 \quad (1)$$

The respective terms describe the upwelling ground radiation, the combination of up- and downwelling canopy radiation, and the sky

Table 1
Overview of meteorological conditions for the Roscommon farm study area on the relevant flight days. $\overline{SM}$ = area-averaged soil moisture ± standard deviation, $T_{IR,av}$ = area-averaged swath-average infrared temperature ± standard deviation, Subscripts 'G' and 'F' denote grass and forest, respectively.

Day	Local time [h]	$\overline{SM_G}$ [m^3m^{-3}]	$\overline{SM_F}$ [m^3m^{-3}]	$T_{IR,av,G}$ [K]	$T_{IR,av,F}$ [K]	Precipitation
1/11	14.35–14.45	0.283 ± 0.028	0.184 ± 0.019	301.88 ± 1.03	302.06 ± 1.20	± 16.5 mm on previous 2 days; 0.4 mm on this day
8/11	10.30–10.40	0.217 ± 0.011	0.127 ± 0.059	300.24 ± 1.56	300.72 ± 1.90	Rain just before flights; previous 2 days dry
10/11	10.10–10.20	0.097 ± 0.002	0.055 ± 0.030	304.73 ± 1.65	305.37 ± 2.08	0.2 mm previous day; 8.8 mm 2 days ago
15/11	10.05–10.15	0.068 ± 0.011	0.035 ± 0.019	312.04 ± 1.59	312.91 ± 1.84	Dry
22/11	10.00–10.10	0.031 ± 0.008	0.014 ± 0.003	313.57 ± 3.11	317.66 ± 2.51	Dry

radiation reflected by the ground surface. The sky radiation reflected by the canopy is neglected, as is multiple scattering between the ground and the canopy. The parameters T_S and T_C are the physical temperatures of the soil and vegetation canopy, respectively. The vegetation canopy can consist of either grass or forest, indicated by the respective subscripts 'G' and 'F' from here onwards. The sky brightness temperature $T_{B,sky}$ is calculated according to the method outlined in (Pellarin et al., 2003). The variable ω^P (P = H or V polarization) is the single scattering albedo of the vegetation layer and the variable $\gamma^{P,\theta}$ (θ = observation angle) describes the transmissivity of the vegetation layer, which is related to vegetation optical depth $\tau^{P,\theta}$ according to:

$$\gamma^{P,\theta} = \exp(-\tau^{P,\theta} / \cos\theta) \tag{2}$$

dividing the optical depth by the cosine corrects for the difference in physical pathway length through the canopy layer at different angles. However, it should be noted that the variables τ and ω in L-MEB are effective parameters resulting from the use of the Delta–Eddington approximation (Joseph et al., 1976), which assumes that scattering is in the forward direction only. Thus, $\tau^{P,\theta}$ in Eq. (2) must account for the fact that in reality the incident radiation comes from a range of directions within the canopy. While in Eq. (2) the cosine is taken of a single angle, in fact the aperture of the radiometer and the structure of the canopy determine the real range of incidence angles.

In order to take into account the effects of canopy anisotropy, an extra parameter (tt^P) has been introduced in the L-MEB model to account for such remaining angular effects. The relation between canopy anisotropy (i.e. structure) effects at V and H polarization is expressed by $rtt = tt^V / tt^H$. The correction using tt^P results in τ_{NAD}, with the subscript 'NAD' denoting theoretical nadir values:

$$\tau^{P,\theta} = \tau_{NAD}(\sin^2(\theta) \cdot tt^P + \cos^2(\theta)) \tag{3}$$

The reflectivity $R_S^{P,\theta}$ of a rough soil is obtained with a semi-empirical approach combining the Fresnel equations with a roughness correction based on the approach in (Wang and Choudhury, 1981):

$$R_S^{P,\theta} = [(1-Q_R) \cdot R{*}_S^{H,\theta} + Q_R \cdot R{*}_S^{V,\theta}] \cdot \exp(-H_R \cdot \cos^{N_R^P}(\theta)) \tag{4}$$

In this equation, $R^*{}_S^{P,\theta}$ is the smooth soil reflectivity calculated from the Dobson dielectric mixing model (Dobson et al., 1985) and the Fresnel equations. H_R and N_R^P are parameters describing the soil effective (topographic and dielectric) roughness and the angular dependency of this roughness, respectively. The parameter Q_R describes polarization mixing and is set to 0 in L-MEB.

An overview of default parameter values for L-MEB is given in Table 2, together with the relevant references.

Table 2

Parameter	Default value	Reference
A. Default values used as input in L-MEB for non-retrieved (i.e. 'fixed') parameters		
tt_F^P	1	Kerr et al., 2007
tt_G^P	1	Kerr et al., 2007
$H_{R,F}$	0.5	Kerr et al., 2007
$H_{R,G}$	0.4	Saleh et al., 2009
N_R^P	1	Wigneron et al., 2007
Q_R	0	Wigneron et al., 2007
Parameter	**Initial value**	**Reference**
B. Initial values used in L-MEB for retrieved parameters		
$\tau_{NAD,F}$	0.45	Grant et al., 2009
$\tau_{NAD,G}$	0.14	Saleh et al., 2007
ω_F^P	0.087	Della Vecchia, Ferrazzoli, et al., 2006
ω_G^P	0.05	Saleh et al., 2007
SM	0.15	–

In this study, an extra (polarization-independent) parameter, denoted β, was introduced in the model to correct for uncertainties resulting from the lack of detailed information on soil physical properties (e.g. field measurements of *SM*, percentages sand and clay, and roughness) and the possibly imperfect choice of dielectric mixing model. Because the parameter β corrects for incomplete information on soil physical properties, which are independent of polarization, β itself was also assumed to be polarization-independent. To this end, the value of rough soil reflectivity calculated in L-MEB was multiplied by β:

$$R_{S,corr}^{P,\theta} = R_S^{P,\theta} \cdot \beta \tag{5}$$

The introduction of this 'correction parameter' β allows the assumption of a correct roughness value in the *SM* retrievals, as will be discussed in more detail in the following paragraph (Section 3.2).

3.2. Retrievals

As stated in Section 2.2, dual-polarized PLMR observations were made at incidence angles of +/−7°, +/−21.5° and +/−38.5°, the six angular footprints together forming one swath. The assumption was made that, within one swath, all forest-covered parts were homogeneous (i.e. they had the same physical properties), and analogously for the grass-covered parts. In some cases angular footprints were missing, therefore only swaths containing more than 2 angular footprints were selected for the retrievals, giving a minimum of 4 and a maximum of 12 observations per swath (i.e. 2 polarizations and 2–6 angles).

The retrieval procedure for L-MEB is based on the minimization of the cost function *CF* shown in Eq. (6):

$$CF = \frac{\sum_1^N (T_B^{\circ} - T_B)^2}{\sigma_{T_B}^2} + \sum_{i=1}^{n} \frac{\sum_1^N (p_i - p_i^{ini})^2}{\sigma_{p_i}^2} \tag{6}$$

The error computed by this cost function represents the sum of the squared differences in observed and simulated brightness temperatures $(T_B{}^\circ - T_B)^2$ plus the squared differences in retrieved and initial parameter values $(p_i - p_i^{ini})^2$ for N observations and n parameters. The parameters $\sigma_{T_B}^2$ and σ_{pi}^2 are the corresponding variances, and allow for the possibility of constraining parameters. However, no constraints were used in the current study (i.e. large values of σ_{pi}^2 were used) and all retrievals were tested for model convergence. Initial values for retrieved parameters are given together with the relevant references in Table 2.

3.2.1. Methodology

First, retrievals over homogeneous swaths were undertaken with field measurements of soil moisture as input, in order to obtain site-specific values of the main L-MEB parameters. Then, retrievals of soil moisture and optical depth were performed over heterogeneous swaths. In both cases it was assumed that physical footprint temperatures T_S and T_C were known, which is also the assumption of the SMOS processor. Non-retrieved parameters were fixed to the default values given in Table 2.

3.2.2. Homogeneous swaths

The retrievals over homogeneous swaths were performed per observation day, per flight line. Homogeneous forest and grass swaths within a given flight line were selected and the assumption was made that all areas of a particular vegetation type (grass or forest) within a given flight line were identical. Then, one single retrieval was performed using all the homogeneous forest swaths of a given flight line, and one using all the homogeneous grass swaths. Note that only four of the six flight lines covered forest areas (cf. Fig. 1). The choice to do the retrievals per flight line rather than for the whole area at once was made in order to obtain a better insight into the spatial variability of the parameters and the errors in their retrieval.

Input values of *SM* were taken from the available field measurements. Swath *SM* was calculated as follows: if a PLMR swath contained Hydraprobe point measurements, the *SM* value for that swath was calculated by taking the average of the ground measurements. However, a majority of the swaths, especially in the forest areas, did not contain any Hydraprobe measurements. In these cases, an 'observed' soil moisture for the swath was calculated as $SM_{swath} = \alpha \cdot \overline{SM_F} + (1-\alpha) \cdot \overline{SM_G}$, with $\overline{SM_F}$ and $\overline{SM_G}$ indicating average forest and grassland soil moisture, respectively. These averages (cf. Table 1) were calculated from all Hydraprobe *SM* measurements in the relevant homogeneous swaths (forest or grassland). An estimate of the errors involved in using the area-averages rather than having exact swath values of *SM* is given by the standard deviations of $\overline{SM_F}$ and $\overline{SM_G}$ in Table 1, which are rather low.

Each of the parameters H_R, N_R^P and tt^P was fixed rather than included in the retrievals because the latter option systematically resulted in model instability, i.e. bad convergence, when tested for each parameter separately. Therefore, the actually retrieved parameters over homogeneous swaths were τ_{NAD}, ω^H, ω^V and β.

By introducing the parameter β in the model (Section 3.1), all errors related to soil emission which can influence retrieval results will be taken into account by β rather than by H_R, which would be the case if the retrievals were performed without β and including H_R. The advantage of this approach becomes apparent in the next step when *SM* is retrieved. Although a date-specific relationship remains between *SM* and β, the retrieved values of *SM* are at least not directly influenced by erroneous values of H_R. The errors in the retrieved values of *SM* will therefore give a better idea of the actual retrieval errors involved, rather than merely being a reflection of errors in the previously retrieved H_R. In other words, the inclusion of the correction parameter β allows the assumption of a correct roughness value in the *SM* retrievals. Indirectly, the parameter β might also partly correct for errors in soil temperature.

3.2.3. Heterogeneous swaths

Retrievals over heterogeneous swaths were performed using the *a priori* information on land cover fractions obtained from the land use map (Section 2.2). In the case of heterogeneous swaths, two modelling approaches were tested: 1) simultaneous retrieval of swath-effective values of soil moisture and optical depth (SM_{swath} and $\tau_{NAD,swath}$), and 2) simultaneous retrieval of grassland soil moisture and optical depth values (SM_G and $\tau_{NAD,G}$). These two methods were chosen in order to show two extremes in the range of possible retrieval configurations consisting of combinations of *SM* and τ_{NAD}.

In the first modelling approach, it was assumed that the soil moisture content under grassland and forest areas was equal, i.e. $SM_{swath} = SM_G = SM_F$. While this assumption is incorrect in reality, it should be kept in mind that the soil emission from forested surfaces is believed to make only a minor contribution to the observed brightness temperature, with the majority of the forest signal coming from the vegetation itself. The errors involved in this approach are therefore less extreme than might be thought.

In this approach, footprint temperature $T_{footprint}$ was approximated by $T_{footprint} = \alpha \cdot T_F + (1-\alpha) \cdot T_G$. Further model inputs were the default parameters given in Table 2 and the daily area-averages of ω^H, ω^V and β taken from the retrievals over homogeneous swaths (previous section).

Model inputs for the second approach differed from those for the first approach in the following ways: SM_F was fixed to the area-average value, $\tau_{NAD,F}$ was fixed to the average daily value resulting from the retrievals over homogeneous swaths (previous section), and T_F and T_G were separate input values. Although this approach is not likely to be implemented operationally due to the unavailability of initial information on the above parameters, the results are included in this study as a theoretical exploration of the hypothesis that 'the soil moisture of the non-forested part of the pixel might still be retrieved with the required accuracy if the emission of the forested part of the pixel is modelled correctly enough'. In theory, the first (swath-effective *SM* retrievals) and second (grassland *SM* retrievals) approaches respectively represent worst- and best-case scenario's in terms of the amount of initial available model input.

It should be specifically noted that model convergence for this second approach was only achieved if a given swath contained at least two angular footprints containing 100% grass cover. The reason for this is, of course, the fact that in order to retrieve two (here: grassland) parameters, at least two independent (grassland) observations are needed. This fact should be kept in mind for any future studies dealing with within-pixel retrievals. As a result of this restriction, there were less heterogeneous swaths available for analysis in the second approach than in the first.

It should be noted that the antenna pattern was not taken into account during the retrievals over heterogeneous swaths, i.e. simulated T_B values were not weighted by the distribution of intensity within the PLMR footprint. However, the resulting errors are negligible; as an indication, a comparison of weighted and non-weighted values of α on 1st Nov. ($N = 1552$) resulted in a correlation coefficient of 0.999 and a root mean square error (RMSE) in α of 0.0268. In other words, at most 2.7% of the swath emission was incorrectly calculated by not taking the antenna pattern into account, while a considerable reduction in computing time was won.

4. Results and discussion

4.1. Footprint temperature and emissivity

4.1.1. Thermodynamic temperatures

Field measurements of temperature were made at one fixed location in the forest and one fixed location in the grassland area (Section 2.2). The field measurements, together with the average T_{IR} value for the corresponding swath, are shown in Table 3. T_F was approximated by taking the average of soil (2 cm depth), bole and canopy temperatures at the forest location, whereas T_G was approximated by soil temperature at 1 cm depth at the grass location. These approximations were justified by the fact that the field measurements of soil and canopy temperatures were very similar (differences in the order of 1.5–3 K). In theory, soil temperatures at depth could also be important in the case of a dry, sandy soil. However, in the NAFE '05 data set the temperature and moisture data necessary for a correct calculation of effective soil temperature were lacking. Given the high spatial variability in temperature, besides the presence of a vegetation cover, neglecting the soil temperature at depth in the overall temperature calculations is not expected to introduce large errors in the resulting patterns of soil moisture retrieval found in this study.

The bias for forest and grassland in Table 3 gives the difference between the thermodynamic temperatures derived from thermal infrared observations ($T_{IR,F}$ and $T_{IR,G}$) and those derived from field measurements (T_F and T_G). It can be seen that in the wettest conditions (1st Nov.), T_F and

Table 3
Thermal infrared (T_{IR}) and field (T) measurements of temperature in a forest (F) and a grassland (G) footprint.

Date	$T_{IR,F}$ [K]	T_F [K]	Bias (F)	$T_{IR,G}$ [K]	T_G [K]	Bias (G)
1st Nov.	302.11	300.85	1.26	302.93	301.05	1.88
8th Nov.	299.57	292.83	6.74	299.28	296.14	3.14
10th Nov.	306.91	296.44	10.47	305.76	299.05	6.71
15th Nov.	309.62	294.25	15.37	313.02	299.05	13.97
22nd Nov.	315.17	294.40	20.77	320.28	301.93	18.35

T_G were very similar at the time of flight. In drier conditions, T_G was generally higher than T_F. Furthermore, in drier conditions the T_{IR}-derived values clearly start to overestimate those derived from field measurements quite substantially, mainly due to the difference in sampling depth between the two methods. Table 3 shows that, for both vegetation types, this overestimation (i.e. the bias) increases almost linearly with time. Besides resulting from the difference in sampling depth, the discrepancies are also partly instrumental in origin. In order to correct for both effects, the thermodynamic temperature ($T_{\text{footprint}}$) of a footprint with a given forest fraction α was calculated as in Eq. (7), using the bias (F) and bias (G) of the observation day in question.

$$T_{footprint} = \alpha \cdot (T_{IR,F} - bias(F)) + (1-\alpha) \cdot (T_{IR,G} - bias(G)) \tag{7}$$

4.1.2. Emissivity

Fig. 2 gives examples of the angular emissivities of homogeneous grassland and forest footprints, respectively, using observations made on 1st and 22nd November, under 'wet' and 'dry' conditions respectively.

Grass and forest emissivities e_G and e_F were calculated according to the Rayleigh–Jeans approximation $(T_B - T_{B,\text{sky}})/(T_{\text{footprint}} - T_{B,\text{sky}})$ (Ulaby et al., 1986) and plotted against incidence angle θ. The patterns seen in Fig. 2 are in agreement with theory, showing increasing and decreasing emissivities with θ for V and H polarization, respectively. This implies that the (polarised) soil emission is only partly attenuated by the vegetation layer. The figures show that, as expected, e_G is slightly lower than e_F, and e_G shows greater angular variation than e_F. The fact that emissivity is higher and the signal is flatter over forested areas indicates a higher vegetation emissivity and a stronger attenuation of the soil signal, and therefore a lower sensitivity to soil moisture changes than in grassland areas.

The difference in emissivity between wet and dry conditions shows that there is a certain sensitivity of above-canopy brightness temperature to changing moisture conditions for open Eucalypt forests. The fact that there is less scatter present in the 'dry' data is most probably due to the inherently high emission from a dry soil, in which case the relative influence of vegetation and surface roughness on the signal becomes smaller, as suggested earlier by (Crosson et al., 2005). Also, soil moisture usually becomes more homogeneous in dry conditions. The few outliers in the data are assumed to be the result of wrongly classified landuse for those footprints.

It was found that in wet conditions the range in brightness temperature was much larger than the range in thermodynamic temperature, indicating a large spatial variation and large effect of non-temperature variables such as canopy parameters, soil moisture and/or effective surface roughness. For dry conditions, the variation in these surface characteristics is clearly smaller and thermodynamic temperature may play a more important role. These conclusions were found to be valid for any given α, i.e. for both homogeneous and heterogeneous footprints.

4.2. Retrievals

4.2.1. Retrievals from homogeneous swaths

The parameter values retrieved from homogeneous swaths are shown in Table 4A (forest) and B (grass). There are differences in parameter values between flight lines, owing to the fact that in reality the vegetation cover is of course not homogeneous, however, although the large spatial variability is visible, the general orders of magnitude remain fairly consistent. The single scattering albedo for H-pol is systematically somewhat higher than for V-pol, while β varies somewhat between flight days, as expected. The negative values of forest single scattering albedo on 8th November could be due to the fact that rainfall occurred just before the flights. This effect is, however, not seen in the grass swaths, where the shorter vegetation might have resulted in the precipitation already having dried up. In further analyses, daily averages of ω_F^H and ω_F^V for 8th

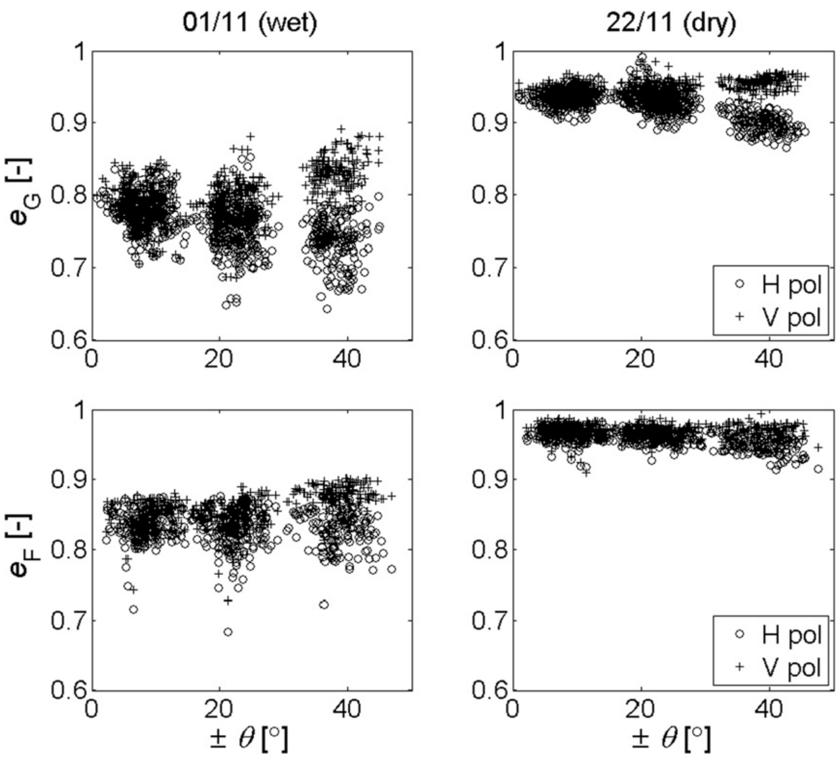

Fig. 2. Example of angular emissivities of (top) 100% grassland footprints (e_G) and (bottom) 100% forest footprints (e_F) under 'wet' (left) and 'dry' (right) conditions on 1st and 22nd Nov. respectively. Corresponding area-average soil moisture values are $SM_G \approx 0.28\ \text{m}^3\text{m}^{-3}$ and $SM_F \approx 0.18\ \text{m}^3\text{m}^{-3}$ (wet) and $SM_G \approx 0.03\ \text{m}^3\text{m}^{-3}$ and $SM_F \approx 0.01\ \text{m}^3\text{m}^{-3}$ (dry).

Table 4

Date	Flightline	N	τ_{NAD}	ω^H	ω^V	β	RMSE (T_B) [K]
A. Retrieved parameter values for homogeneous forest swaths (N = number of swaths)							
1/11	1	103	0.47	0.02	0.02	2.66	7.688
	2	161	0.35	0.06	0.05	1.83	6.321
	3	153	0.36	0.04	0.03	1.93	6.911
	4	130	0.45	0.04	0.03	2.31	5.894
8/11	1	107	0.36	0.00	−0.01	1.89	6.550
	2	185	0.38	−0.01	−0.03	1.93	6.795
	3	171	0.46	0.01	−0.00	2.27	6.720
	4	120	0.47	−0.01	−0.02	2.33	5.328
10/11	1	125	0.63	0.04	0.04	3.76	6.127
	2	119	0.48	0.04	0.04	2.58	6.704
	3	155	0.54	0.06	0.05	2.86	5.592
	4	97	0.52	0.03	0.04	2.90	4.911
15/11	1	93	0.50	0.05	0.04	1.83	3.289
	2	103	0.46	0.05	0.04	1.67	4.760
	3	169	0.43	0.05	0.04	1.54	4.668
	4	95	0.52	0.05	0.04	1.79	3.245
22/11	1	88	0.66	0.04	0.03	2.46	3.977
	2	164	0.35	0.08	0.06	1.06	4.502
	3	144	0.78	0.03	0.02	3.34	3.986
	4	128	0.76	0.03	0.03	3.19	4.204
B. Retrieved parameter values for homogeneous forest swaths (N = number of swaths)							
1/11	1	198	0.39	0.02	0.02	1.88	6.368
	2	184	0.36	0.05	0.04	1.67	6.442
	3	106	0.34	0.05	0.04	1.54	7.687
	4	95	0.23	0.05	0.03	1.26	7.320
	5	100	0.23	0.14	0.11	1.20	9.681
	6	68	0.28	0.09	0.07	1.32	9.361
8/11	1	215	0.39	0.04	0.03	1.58	5.242
	2	165	0.34	0.05	0.03	1.41	6.090
	3	134	0.23	0.05	0.03	1.16	7.206
	4	122	0.28	0.02	0.01	1.42	9.061
	5	110	0.26	0.06	0.04	1.24	8.166
	6	96	0.23	0.05	0.04	1.13	7.588
10/11	1	205	0.58	0.06	0.06	2.76	4.310
	2	165	0.52	0.06	0.06	2.36	5.371
	3	140	0.42	0.09	0.09	1.93	6.649
	4	101	0.41	0.11	0.10	1.93	7.645
	5	64	0.21	0.16	0.15	1.26	6.703
	6	48	0.30	0.10	0.10	1.50	7.509
15/11	1	247	0.41	0.06	0.05	1.21	4.179
	2	159	0.37	0.09	0.08	0.96	4.136
	3	120	0.59	0.06	0.05	1.59	4.540
	4	113	0.38	0.08	0.07	1.13	5.758
	5	127	0.31	0.08	0.07	0.93	4.585
	6	45	0.48	0.09	0.07	1.02	4.285
22/11	1	215	0.26	0.08	0.08	0.97	4.382
	2	162	0.65	0.05	0.04	2.12	4.402
	3	113	0.77	0.05	0.04	2.51	3.992
	4	108	0.62	0.06	0.05	1.53	4.255
	5	110	0.72	0.05	0.04	2.29	4.184
	6	51	0.22	0.09	0.08	0.88	4.259

November were therefore estimated by taking the averages of the 1st and 10th November, i.e. the observation days before and after Nov. 8th. Both forests and grass show high retrieved values of either τ_{NAD} (especially) or ω^P on 22nd of November, the reason for which is not well understood. The values of β are reasonable given the low reflectivity of a sandy soil and the physical condition $0<R^{P,\theta}_{S,corr}\cdot\beta<1$ was valid in all cases. In fact, the reflectivity values of this rather dry sandy soil were very low, and so even the larger values of β still result in a rather low reflectivity. Given the soil type and conditions, it is believed that the rather varied values of β partly reflect volume scattering within the soil. In addition, at low moisture levels the dielectric constant has a reduced sensitivity in response to changes in soil moisture content. It may be possible that the choice of the Dobson dielectric mixing model in L-MEB is not the most appropriate under this type of conditions, an issue which is currently under research.

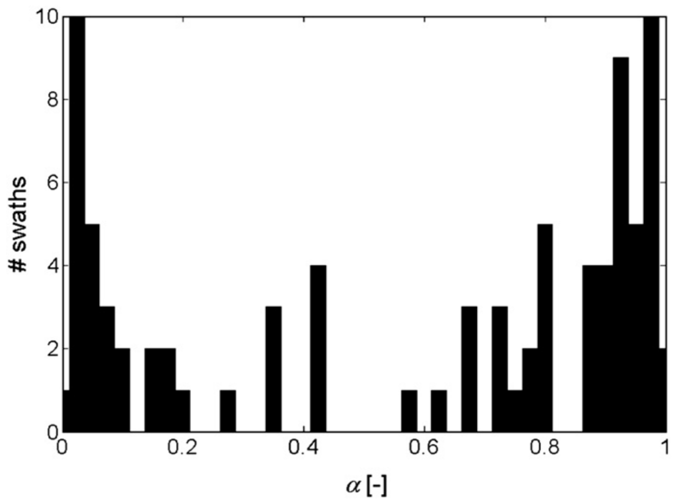

Fig. 3. Example of the distribution of forest fraction α for 375 m by 62.5 m heterogeneous swaths ($0.01<\alpha<0.99$) in the Roscommon farm area on 1st November.

4.2.2. Retrievals from heterogeneous swaths

In order to give an idea of the distribution of forest fraction α per swath, the histogram in Fig. 3 shows an example for the 1st November. Note that only heterogeneous swaths ($0.01<\alpha<0.99$) have been included in the figure. The distribution varies slightly per observation day, but the overall pattern is very similar in all cases. The total number of 87 heterogeneous swaths was relatively small, as the forested parts of Roscommon were not very extensive. In comparison, there were 185 homogeneous grass swaths ($\alpha<0.01$) and 98 homogeneous forest swaths for this day.

The results of the retrievals from heterogeneous swaths ($0.01\leq\alpha\leq0.99$) are shown in Table 5A,B, and Fig. 4. Table 5A shows the results for the first retrieval approach, i.e. simultaneous retrieval of SM_{swath} and $\tau_{NAD,swath}$. It can be seen that, except on the driest day, the average retrieved SM_{swath} slightly overestimates the average observed value, which was an effect also found for pixels in (Loew, 2008). On the other hand, the high standard deviation of the retrievals seems to reflect the actual spatial variability, which is much higher than that of the observations. The field observed standard deviation, however, is based on only a few measurements, insufficient to characterize the actual spatial variability. It should also be realized that, in this case, the retrieved values refer to 'swath-effective' values of which the exact physical meaning is difficult to identify because of non-linear mixing effects, and because the soil properties between the forest and the grass soils are different.

As indicated in the study by Loew (2008), it is important to observe the bias in SM together with the RMSE, as a low RMSE can still be coupled to a high bias. In the current study it should be kept in mind that, due to the limited number of field observations, many of the observed values of SM_{swath} are based on α-weighted area-averages and great caution should thus be taken with the interpretation of RMSE(SM_{swath}) and bias (SM_{swath}).

The retrieved values of $\tau_{NAD,swath}$ are slightly higher than expectations based on Table 4A,B, an effect which will be discussed later in more detail in the context of Fig. 4. Finally, the values of RMSE (T_B) indicate that, overall, the model is able to match T_B simulations to observations reasonably well, although this of course becomes more difficult with increasing wetness, when soil and vegetation emission show increasingly opposed behaviour (i.e. soil emission decreases while vegetation emission increases).

The results for 1st November (wet) and 22nd November (dry) are shown in more detail in Fig. 4 (note that y-axis scales differ) using the first retrieval approach, i.e. simultaneous retrieval of SM_{swath} and

Table 5

Date	N	SM_{swath} (ret)	SM_{swath} (obs)	RMSE (SM_{swath})	Bias (SM_{swath})	$\tau_{NAD,swath}$ (ret)		RMSE (T_B)
A. Results of SM_{swath} and $\tau_{NAD,swath}$ (method 1) retrievals from heterogeneous swaths ($0.01 \le \alpha \le 0.99$). N = number of swaths, with number of removed outliers in parentheses. Retrieved and observed values indicated by 'ret' and 'obs', respectively. Values shown are average +/− standard deviation swath soil moisture (SM_{swath} [m^3m^{-3}]), root mean square error (RMSE) and bias between retrieved and observed SM_{swath}, average +/− standard deviation swath optical depth ($\tau_{NAD,swath}$ [−]), and the RMSE in brightness temperature (T_B [K])								
1/11	81 (6)	0.27 ± 0.12	0.23 ± 0.05	0.13	0.04	0.47 ± 0.20		3.798
8/11	97 (12)	0.17 ± 0.12	0.17 ± 0.03	0.10	0.01	0.50 ± 0.21		4.623
10/11	82 (3)	0.09 ± 0.09	0.07 ± 0.02	0.09	0.02	0.68 ± 0.28		3.007
15/11	69 (7)	0.07 ± 0.06	0.05 ± 0.01	0.07	0.02	0.68 ± 0.37		2.013
22/11	80 (3)	0.01 ± 0.03	0.02 ± 0.01	0.03	−0.01	0.73 ± 0.29		1.611
Date	N	SM_G (ret)	SM_G (obs)	RMSE (SM)	Bias (SM)	$\tau_{NAD,G}$ (ret)	$\tau_{NAD,G}$ (obs)	RMSE (T_B)
B. Results of SM_G and $\tau_{NAD,G}$ (method 2) retrievals from heterogeneous swaths ($0.01 \le \alpha \le 0.66$). N = number of swaths, with number of removed outliers in parentheses. Retrieved and observed values indicated by 'ret' and 'obs', respectively. Values shown are average +/− standard deviation grassland soil moisture (SM_G [m^3m^{-3}]), root mean square error (RMSE) and bias between retrieved and observed SM_G, average +/− standard deviation grassland optical depth ($\tau_{NAD,G}$ [−], observed values from Table 4B), and the RMSE in brightness temperature (T_B [K])								
1/11	22 (8)	0.24 ± 0.13	0.29 ± 0.01	0.13	−0.05	0.26 ± 0.15	0.30 ± 0.07	3.776
8/11	35 (5)	0.24 ± 0.15	0.21 ± 0.01	0.15	0.03	0.33 ± 0.19	0.29 ± 0.07	3.582
10/11	26 (5)	0.09 ± 0.06	0.09 ± 0.01	0.06	−0.00	0.44 ± 0.20	0.41 ± 0.14	3.383
15/11	18 (8)	0.05 ± 0.03	0.07 ± 0.01	0.03	−0.02	0.39 ± 0.28	0.42 ± 0.10	1.999
22/11	17 (10)	0.02 ± 0.02	0.03 ± 0.01	0.02	−0.01	0.35 ± 0.32	0.54 ± 0.24	1.272

$\tau_{NAD,swath}$. Results are presented as averages ± 75th percentile for 0.2 increments in α. The choice to use percentiles instead of standard deviation was based on the skewed distribution of the results. If no error bars are present in the figure, the number of swaths in that class was too small to allow it. Although Fig. 4 does also reflect the large amount of spatial variability in the data, due to the variability in field conditions and the many uncertainties involved in the analysis, the general patterns are clear. The retrieved values of $\tau_{NAD,swath}$ show, as expected, a generally increasing pattern with increasing forest fraction α. Excepting the outlier on 22nd Nov., the values of $\tau_{NAD,swath}$ for low α are of the same order of magnitude as those found for grassland areas in Table 4B. However, the values of $\tau_{NAD,swath}$ for higher α are higher than would be expected according to Table 4A and it thus appears that increased forest fraction does influence retrievals of optical depth by resulting in an increased overestimation.

The retrieved values of SM_{swath} in the right-hand images show maximum values of retrieved SM_{swath} at intermediate α. Even though these plots do not show the actual errors in retrieved SM (because, as said previously, values of RMSE(SM_{swath}) are not completely reliable), an idea of the errors involved can be derived from subtracting the area-average observed SM (the middle of the two solid lines) from the retrieved values. In this case, an approximately convex curve remains.

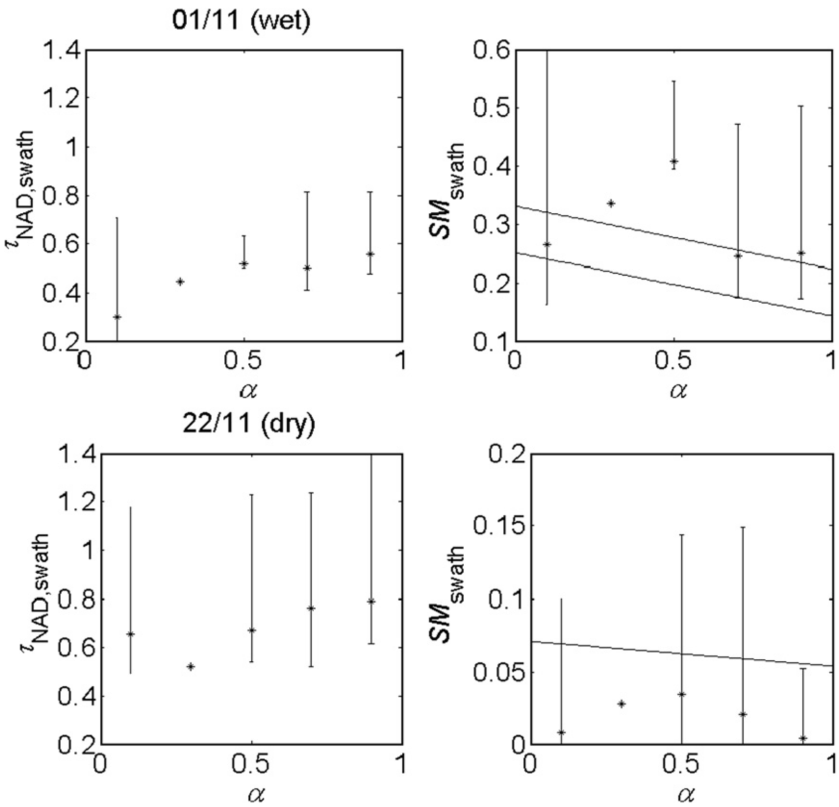

Fig. 4. Retrieved 'swath-effective' values of soil moisture (SM_{swath} [m^3m^{-3}]) and optical depth ($\tau_{NAD,swath}$ [−]) plotted against forest fraction α for heterogeneous swaths ($0.01 \le \alpha \le 0.99$) on (top) 1st November (wet) and (bottom) 22nd November (dry). Left: average and 75th percentile of retrieved $\tau_{NAD,swath}$. Right: average and 75th percentile of retrieved SM_{swath}. Solid lines indicate area-average $SM(= \alpha \cdot \overline{SM_F} + (1-\alpha) \cdot \overline{SM_G}) \pm 0.04\ m^3m^{-3}$ (with $\overline{SM_F}$ and $\overline{SM_G}$ from Table 1). NB. Note different ranges of y-axes in right-hand plots.

Such a shape was also found in a modelling study by Van de Griend et al. (2003) for retrievals over pixels containing a mix of bare soil ($\tau=0$) and vegetation with $\tau=0.4$. That study also found a flatter curve in drier conditions, as seen here in Fig. 4. However, contrary to the current study, the modelling study assumed that no *a priori* knowledge of α was available. Another modelling study by Loew (2008) which did assume *a priori* knowledge of α to be available, shows a result for mixed forest/grassland pixels which could be interpreted as a similar curved shape, although it is not conclusive as forest fractions above 65% are sparse. However, that study assumed higher values of forest optical depth ($\tau=0.8$–1) than the current study does. It seems that the mix of optical depth values, i.e. the contrast present between forested and non-forested areas, determines the shape of the curve, whereas the un-/availability of *a priori* knowledge of α mainly influences the absolute error values. Modelling studies by Van de Griend et al. (2003, 2004) both with and without *a priori* knowledge of α, show that when higher values of τ are introduced in the mixed pixel, the maximum of the error curve shifts towards higher values of α. It is therefore too general a statement to simply say that if α is known *a priori*, all pixels containing more than 50% forest fraction will give errors in retrieved *SM* greater than 0.04 m^3m^{-3}. The value of α at which this 0.04 m^3m^{-3} boundary will be crossed (if it is crossed) will differ according to the different land use optical depths within the pixel and their values relative to each other. This makes sense, as optical depth and soil moisture are indirectly linked in the tau–omega model. Unfortunately, the consequence for SMOS is that it will be extremely difficult to find reliable flags for the maximum allowed forest fraction in mixed pixels.

Table 5B shows the results for the second retrieval approach, i.e. simultaneous retrieval of SM_G and $\tau_{NAD,G}$ while the emission of the forested part of the swath is modelled with parameter values as retrieved from the homogenous forest parts. The table shows that in dry conditions the results are generally very reasonable. The results will, at least partly, reflect a compensation for the forward modelled emission of the forested part of the swath. Retrieved values of $\tau_{NAD,G}$ are generally close to observed values (taken from Table 4B), except for 22nd Nov. which had very high values of 'observed' $\tau_{NAD,G}$ (Table 4B). No relationship can be seen between moisture conditions and the degree of over- or underestimation in $\tau_{NAD,G}$. As also said for Table 5A, the values of RMSE(SM_G) and bias(SM_G) should be taken with extreme caution. The study by Loew (2008) found that the bias (*SM*) increases with increasing dryness, therefore the low error values for dry conditions found in the current study should not lead straight to the conclusion that *SM* retrievals over forested areas are reliable enough as long as the moisture content is low. This issue is important for SMOS and deserves further attention in future.

Values and patterns of RMSE(T_B) are very similar to those in Table 5A, therefore it can be concluded that the model does not have more difficulty in fitting simulations to observations when the forest part of the swath emission is known from forward modelling.

It should be noted here that, as explained in §3.2, this second approach only works for swaths with more than 2 angular footprints containing 100% grass. As in this study a maximum of 6 angles was observed for each swath, the consequence of this requirement is that at least 33% of the swath will cover grassland. Therefore, this analysis only includes swaths with $\alpha<0.66$ and a possible heightened influence of high forest fraction is thus not taken into account. Due to this limited range of α and, as a result, the low number of suitable swaths, a figure similar to Fig. 4 was not drawn up for this retrieval approach (retrieval of SM_G and $\tau_{NAD,G}$).

4.3. Effects of errors in L-MEB parameter values

In order to determine the effect of each fixed model parameter on RMSE(*SM*), a sensitivity analysis was performed. Simultaneous retrievals of SM_{swath} and $\tau_{NAD,swath}$ were performed for heterogeneous swaths ($0.01\leq\alpha\leq0.99$), each time with errors superimposed on one of the fixed L-MEB parameters, for 1st November (wet) and 22nd November (dry).

The resulting difference δ(RMSE(SM_{swath})) between the mean RMSE(SM_{swath}) values found for the 'error' and the 'default' situations is plotted *vs.* α for each parameter in Figs. 5 (wet) and 6 (dry), with values of RMSE(SM_{swath}) averaged per 0.2 increment in α. Note that the scales on the *y*-axis can differ per parameter. The specific values of each superimposed error are shown in the figure caption. It should be specifically noted here that the goal of this analysis is not to compare the relative effects of the different model parameters. This is impossible as the effect of each parameter is dependent on the given model configuration. The main focus of this analysis is on the difference in patterns between dry and wet conditions, for different forest fractions ($0\leq\alpha\leq1$). The superimposed errors were based on realistic ranges in parameter values, known from the literature and various SMOS-related studies (e.g. Wigneron et al., 2007 and Kerr et al., 2007).

Figs. 5 and 6 show that the effects of superimposed errors are much more obvious in wet conditions than in dry. In each plot, the difference between two markers indicates, for a given α, the sensitivity of the model to the parameter concerned. In wet conditions (Fig. 5), it can be seen that the effects of temperature T ($T=T_S=T_C$) and the roughness parameters H_R and $N_R^{H,V}$ are greatest in the case of the most highly mixed swaths (i.e. intermediate values of α). The parameters ω^V and tt^V also show the greatest effect on *SM* retrievals in the case of highly mixed swaths, whereas ω^H shows the most effect in more homogeneous grass or forest areas and tt^H shows no clear relationship with α. It is thus quite possible that the greater errors in retrieved SM_{swath} at intermediate α are caused by non-linear mixing effects of (most of) the model parameters. However, in dry conditions (Fig. 6) the effects of superimposed errors are less clearly concentrated at intermediate values of α. As said previously (Section 4.1), in dry conditions the difference between vegetation and soil emission is smaller, therefore it is not surprising that in this case the influence of α on the overall results is also smaller.

Besides the dependence on α, it is obvious that erroneous values of the default L-MEB parameters can lead to high errors in retrieved *SM*, especially in wet conditions. Given the difficulty of determining several of the L-MEB parameters (e.g. tt^P, H_R and N_R^P) independently, this issue will need attention from the very operational start of SMOS. Ideally, these parameters should be determined at the satellite scale by model inversion using actual SMOS data where possible.

5. Summary and conclusions

The NAFE '05 experimental data set was used to investigate L-MEB soil moisture retrievals over mixed *Eucalypt* forest/grassland swaths. Airborne L-band observations were selected over swaths with varying fractions of forest cover (0–1), on five separate days with different moisture conditions. The data set was used to study the retrieval of soil moisture from heterogeneous swaths using two different approaches, both based on *a priori* knowledge of forest fraction (α). Model inputs for non-retrieved parameters were either default values taken from the literature or site- and time-specific values obtained from observations of nearby homogeneous swaths gathered during the same flight. Because of the experiment-specific configuration, the swath was used as the basic calculation unit.

In the first retrieval approach, swath-effective values of soil moisture (*SM*) and swath-effective vegetation optical depth (τ_{NAD}) were simultaneously retrieved using the L-MEB model. In the second approach, soil moisture and optical depth retrievals of the non-forested (i.e. grass) fraction of the swath were performed, while the forest contribution to swath emission was known from forward modelling. This is, to our knowledge, the first study to use experimental data rather

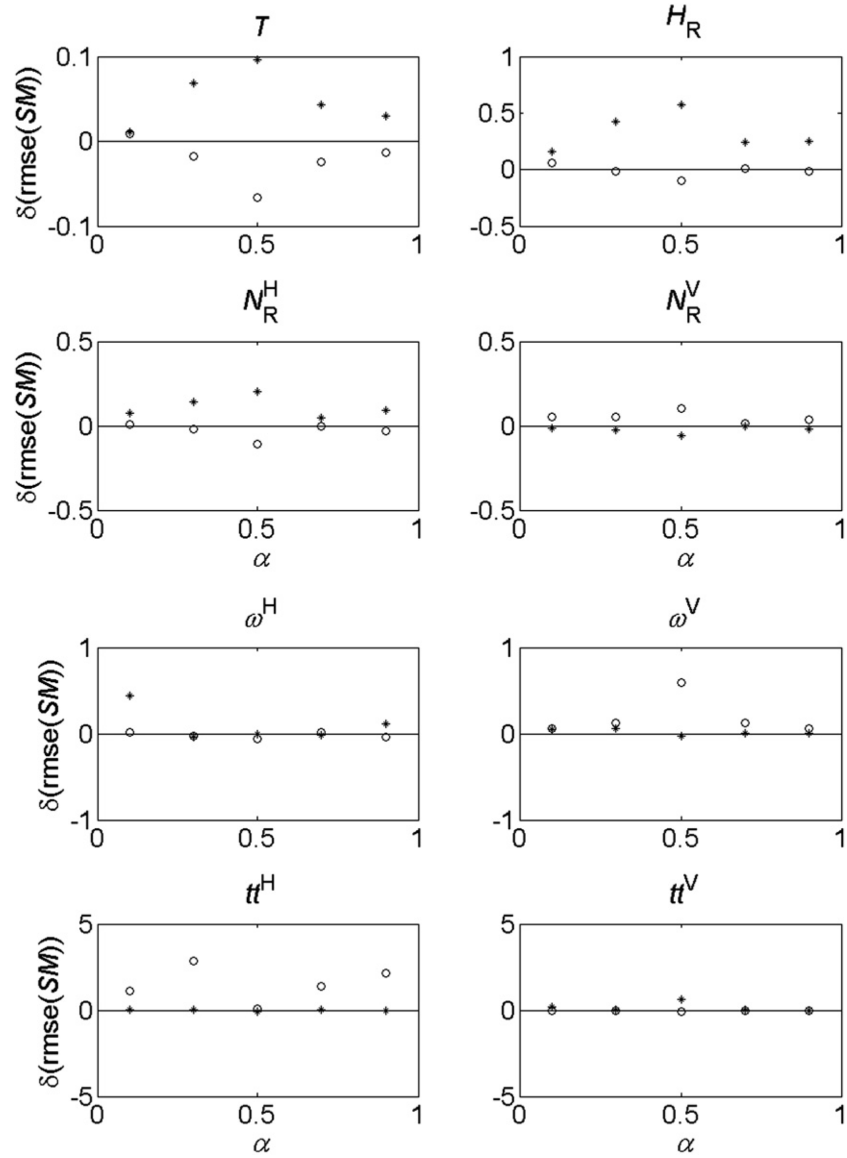

Fig. 5. Results of superimposing errors on each of the fixed L-MEB parameters for 1/11 (wet conditions), then simultaneously retrieving SM_{swath} and $\tau_{NAD,swath}$ for heterogeneous swaths ($0.01 \leq \alpha \leq 0.99$) only. The vertical axis shows the difference (δ [m^3m^{-3}]) between the mean RMSE(SM_{swath}) found with and without (cf. Table 5A) superimposed errors. Legend per focus parameter: T: 'o' = default − 5 K, '*' = default + 5 K; H_R: 'o' = H_R = 0, '*' = default + 0.5; N_R^P: 'o' = default − 1, '*' = default + 1; ω^P: 'o' = ω^P = 0, '*' = default + 0.1; and tt^P: 'o' = default − 0.5, 'Δ' = default + 0.5. All non-focus parameters were fixed to default values during the retrievals. NB. Y-axes differ in range.

than model simulations to specifically investigate the effect of forest cover fraction on soil moisture retrievals.

Because of the large spatial variation within the NAFE '05 experimental site, and the (375 m) resolution of the airborne swaths, a large amount of variation was present in the observed brightness temperatures. Although the amount of ground measurements was limited and the data set showed a few systematic inconsistencies, some additional calibration steps were performed to limit the consequences of these issues, resulting in a consistent data set suitable for the anticipated study. Given the obvious and well known difficulties and limitations of airborne campaigns, the retrieval results were generally very reasonable.

Concerning the swath-effective retrievals, values of swath-effective soil moisture (SM_{swath}) were slightly overestimated compared to area-averaged SM values resulting from field measurements. Retrieved values of $\tau_{NAD,swath}$ showed a general increase with increasing forest fraction (α), as expected, but also an increasing overestimation with increasing forest fraction. Maximum retrieved values of SM_{swath}, and maximum errors in the retrieved values were found at intermediate values of forest fraction. These results are important for the SMOS mission as they indicate the difficulty in flagging upper limits of pixel forest fraction during soil moisture retrievals. The upper limit is expected to differ depending on forest type and density.

A subsequent sensitivity analysis for all L-MEB parameters showed that, especially in wet conditions, the errors superimposed on the parameter values often also had the greatest effect on retrieved SM_{swath} at intermediate values of forest fraction. Besides this, it was shown that erroneous values of the default L-MEB parameters can lead to high errors in retrieved SM, especially in wet conditions. At the SMOS scale, it will therefore be necessary to determine correct parameter values with actual SMOS data and model inversion.

Concerning the retrievals for the non-forested (in this case: grass) swath fractions, SM_G and $\tau_{NAD,G}$ were retrieved simultaneously, with a known forest emission derived from the homogeneous forest swaths in the area. Although these analyses were only valid for the range $0 \leq \alpha \leq 0.6$, retrieved values of SM_G and $\tau_{NAD,G}$ were generally

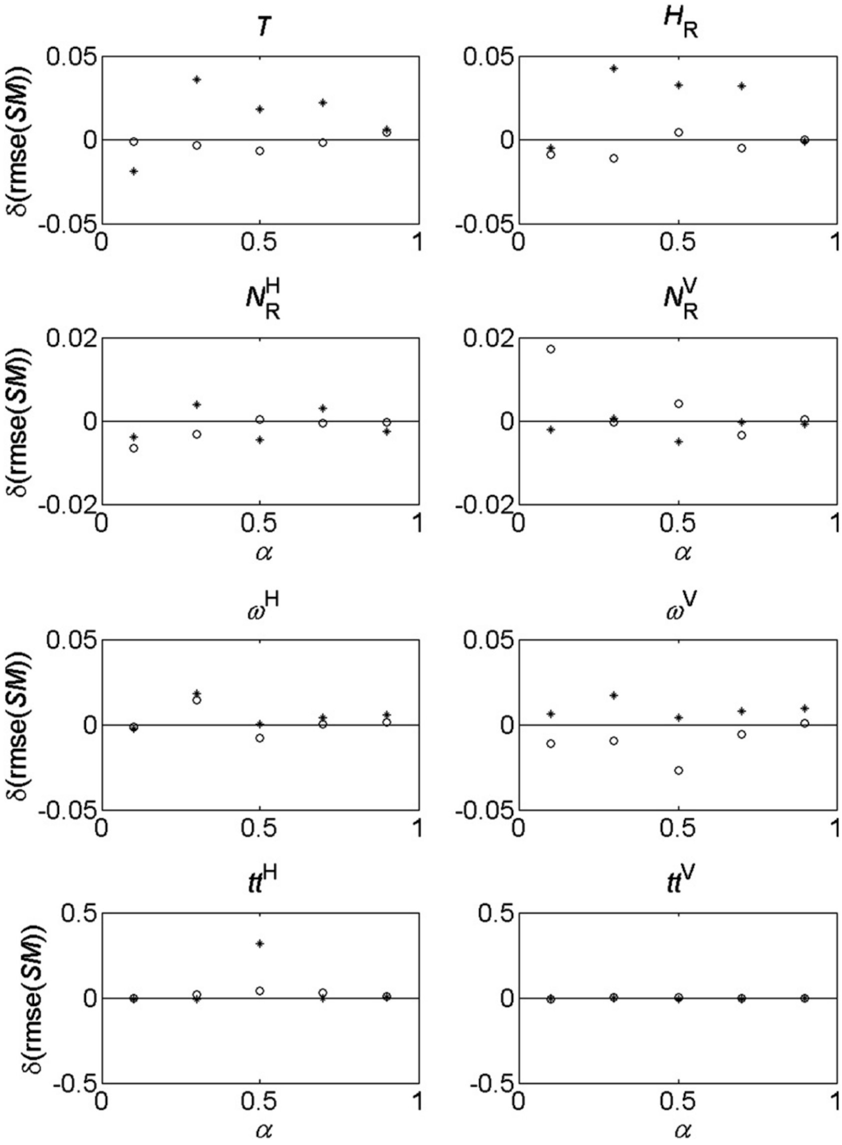

Fig. 6. As for Fig. 5, but for 22/11 (dry conditions).

reasonable and close to observed values. The procedure used in this study, which involves retrievals of canopy parameters over homogeneous swaths, followed by retrievals of *SM* and τ_{NAD} over heterogeneous swaths, can also be used when SMOS is operational.

Due to the use of experimental data focussed specifically on forests, the current study is the first to give a realistic idea of the errors and uncertainties involved in soil moisture retrievals from partly forested swaths. This is a relevant contribution to the analysis of heterogeneous pixels in future studies in general, and to studies concerning SMOS calibration and validation in particular. However, it should be kept in mind that the field experiment on which this study is based was conducted over a rather open Eucalypt forest, and the results presented in this study are therefore site-specific. Of course *Eucalypt* forest is dominant in Australia but much less so in other parts of the world. An interesting follow-up to this study would therefore be to perform similar analyses over a variety of forest structures (i.e. types) and densities, in order to obtain a better idea of the differences in results involved on a global scale. Such a study could also offer more information on the relative influences of forest structure and forest density on soil moisture retrievals. For example, it may turn out that knowledge of the type of forest present in a SMOS pixel is less important for accurate soil moisture retrievals than information on the forest density. This remains to be investigated.

Acknowledgements

First of all, many thanks to the O'Brien family of Roscommon farm for making their property available as part of the NAFE '05/CoSMOS field experiments, and to all the participants of these experiments for the data collection and collaboration. Special thanks also go to Prof. Dr. Jetse Kalma and his wife Martine; to Jetse for making the forest ground measurements possible by arranging the necessary logistics, and to Martine for sharing her extensive knowledge of the Australian vegetation and countryside. Finally, many thanks to Prof. Dr. G. Pegram of the University of KwaZulu-Natal for his help with calculating the PLMR antenna pattern.

This research was funded by NWO, the Netherlands Organisation for Scientific Research and SRON, the Netherlands Institute for Space Research. The main author's participation in the NAFE '05 field experiment and an additional stay at the University of Melbourne were funded with grants from the European Space Agency (ESA) and the VUA-FALW Promovendifonds, respectively. The NAFE campaign was made possible through Australian Research Council Discovery Grant DP0557543.

References

Chauhan, N., Le Vine, D., & Lang, R. (1999). Passive and active microwave remote sensing of soil moisture under a forest canopy. *Proceedings of IGARSS*, *1999*(4), 1914−1916.

Crosson, W., Limaye, A. S., & Laymon, C. A. (2005). Parameter sensitivity of soil moisture retrievals from airborne L-band radiometer measurements in SMEX02. *IEEE Transactions on Geoscience and Remote Sensing*, *43*(7), 1517−1528.

Della Vecchia, A., Ferrazzoli, P., Giorgio, F., & Guerriero, L. (2006). A large scale approach to estimate L band emission from forest covered surfaces. In José A. Sobrino (Ed.), *Second recent advances in quantitative remote sensing* (pp. 925−930). Universitat de Valencia: Servicio de Publicaciones.

Della Vecchia, A., Saleh, K., Ferrazzoli, P., Guerriero, L., & Wigneron, J. -P. (2006). Simulating L-band emission of coniferous forests using a discrete model and a detailed geometrical representation. *IEEE Geoscience and Remote Sensing Letters*, *3*(3), 364−368.

Dobson, M. C., Ulaby, F. T., Hallikainen, M. T., & El-Rayes, M. A. (1985). Microwave dielectric behaviour of wet soil — Part II: Dielectric mixing models. *IEEE Transactions on Geoscience and Remote Sensing*, *23*, 35−46.

Grant, J. P., Saleh, K., Wigneron, J. -P., Guglielmetti, M., Kerr, Y., Schwank, M., Skou, N., & Van de Griend, A. A. (2008). Calibration of the L-MEB model over a coniferous and a deciduous forest. *IEEE Transactions on Geoscience and Remote Sensing*, *46*(3), 808−818.

Grant, J. P., Van de Griend, A. A., Schwank, M., & Wigneron, J. -P. (2009). Observations and modelling of a Pine Forest Floor at L-band. *IEEE Transactions on Geoscience and Remote Sensing*, *47*(7–1), 2024−2034.

Grant, J. P., Wigneron, J. -P., Van de Griend, A. A., Kruszewski, A., Schmidl Søbjærg, S., & Skou, N. (2007). A field experiment on microwave forest radiometry: L-band signal behaviour for varying conditions of surface wetness. *Remote Sensing of Environment*, *109*(1), 10−19.

Guglielmetti, M., Schwank, M., Mätzler, C., Oberdörster, C., Vanderborght, J., & Flühler, H. (2007). Measured microwave radiative transfer properties of a deciduous forest canopy. *Remote Sensing of Environment*, *109*(4), 523−532.

Guglielmetti, M., Schwank, M., Mätzler, C., Oberdörster, C., Vanderborght, J., & Flühler, H. (2008). FOSMEX: Forest soil moisture experiments with microwave radiometry. *IEEE Transactions on Geoscienxe and Remote Sensing*, *46*(3), 727−735.

Hallikainen, M., Jääskeläinen, V. S., Pulliainen, J., & Koskinen, J. (2000). Transmissivity of boreal forest canopies for microwave radiometry of snow. *Proceedings of IGARSS*, *2000*(4), 1564−1566.

Joseph, J. H., Wiscombe, W. J., & Weinman, J. A. (1976). The Delta-Eddington approximation for radiative flux transfer. *Journal of the Atmospheric Sciences*, *33*, 2452−2459.

Kerr, Y. H., Waldteufel, P., Richaume, P., Davenport, I., Ferrazzoli, P., & Wigneron, J. -P. (2007). SMOS level 2 processor for soil moisture, algorithm theoretical based document (ATBD). *CESBIO, IPSL-Service d'Aéronomie, INRA-EPHYSE, Reading University, Tor Vergata University. SO-TN-ESL-SM-GS-0001 Issue 3.a, 05/12/2007*.

Kerr, Y. H., Waldteufel, P., Wigneron, J. -P., Martinuzzi, J. -M., Font, J., & Berger, M. (2001). Soil moisture retrieval from space: The soil moisture and ocean salinity (SMOS) mission. *IEEE Transactions on Geoscience and Remote Sensing*, *39*(8), 1729−1735.

Kirdyashev, K. P., Chukhlantsev, A. A., & Shutko, A. M. (1979). Microwave radiation of the earth's surface in the presence of vegetation cover. *Radiotekhnika*, *24*, 256−264.

Lang, R. H., Chauhan, N., Utku, C., & Le Vine, D. M. (2006). L-band active and passive sensing of soil moisture through forests. *Proceedings of IEEE MicroRad*, *2006*, 193−196.

Lang, R. H., Utku, C., De Matthaeis, P., Chauhan, N., & Le Vine, D. M. (2001). ESTAR and model brightness temperatures over forests: Effects of soil moisture. *Proceedings of IGARSS 2001, IEEE International*, *3*, 1300−1302.

Loew, A. (2008). Impact of surface heterogeneity on surface soil moisture retrievals from passive microwave data at the regional scale: The Upper Danube case. *Remote Sensing of Environment*, *112*, 231−248.

Merlin, O., Walker, J. P., Panciera, R., Young, R., Kalma, J. D., & Kim, E. J. (2007). Calibration of a soil moisture sensor in heterogeneous terrain with the National Airborne Field Experiment (NAFE) data. *Proceedings of MODSIM 2007 International congress on modelling and simulation. Modelling and Simulation Society of Australia and New Zealand, December 2007*.

Mo, T., Choudhury, B. J., Schmugge, T. J., Wang, J. R., Jackson, T. J., Mo, T., Choudhury, B. J., Schmugge, T. J., Wang, J. R., & Jackson, T. J. (1982). A model for microwave emission from vegetation-covered fields. *Journal of Geophysical Research*, *87*(C13), 11229−11237.

Panciera, R., Walker, P., Kalma, J. D., Kim, E. J., Hacker, J., Merlin, O., Berger, M., & Skou, N. (2008). The NAFE'05/CoSMOS data set: Towards SMOS soil moisture retrieval, downscaling and assimilation. *IEEE Transactions on Geoscience and Remote Sensing*, *46*(3), 736−745.

Pardé, M., Wigneron, J. -P., Chanzy, A., Kerr, Y. H., Calvet, J. -C., Waldteufel, P., Schmidl Søbjærg, S., & Skou, N. (2004). N-parameter retrievals from L-band microwave measurements over a variety of agricultural crops. *IEEE Transactions on Geoscience and Remote Sensing*, *42*(6), 1168−1178.

Pellarin, T., Wigneron, J. -P., Calvet, J. -C., Berger, M., Douville, H., Ferrazzoli, P., Kerr, Y. H., Lopez-Baeza, E., Pulliainen, J., Simmonds, L., & Waldteufel, P. (2003). Two-year global simulation of L-band brightness temperatures over land. *IEEE Transactions on Geoscience and Remote Sensing*, *41*(9), 2135−2139.

Rüdiger, C., Hancock, G., Hemakumara, H. M., Jacobs, B., Kalma, J. D., Martinez, C., Thyer, M., Walker, J. -P., Wells, T., & Willgoose, G. R. (2007). Goulburn River experimental catchment data set. *Water Resources Research*, *43*(10), W10403. doi:10.1029/2006WR005837.

Saleh, K., Kerr, Y., Richaume, P., Escorihuela, M., Panciera, R., Delwart, S., Boulet, G., Maisongrande, P., Walker, J. P., Wursteisen, P., & Wigneron, J. -P. (2009). Soil moisture retrievals at L-band using a two-step inversion approach (COSMOS/NAFE'05 Experiment). *Remote Sensing of Environment*, *113*(6), 1304−1312.

Saleh, K., Wigneron, J. -P., Waldteufel, P., De Rosnay, P., Schwank, M., Calvet, J. -C., & Kerr, Y. H. (2007). Estimates of surface soil moisture over grass covers using L-band radiometry. *Remote Sensing of Environment*, *109*(1), 42−53.

Ulaby, F., Moore, R. and Fung, A. (1986). Microwave remote sensing: Active and passive, Vol. III: from theory to applications. (pp. 200–201; 1537–1539). Artech House, Dedham, MA.

Van de Griend, A. A., Wigneron, J. -P., & Waldteufel, P. (2003). Consequences of surface heterogeneity for parameter retrieval from 1.4 GHz multiangle SMOS observations. *IEEE Transactions on Geoscience and Remote Sensing*, *41*(4), 803−811.

Van de Griend, A. A., Wigneron, J. -P., & Waldteufel, P. (2004). Soil moisture retrieval from heterogeneous surfaces by 1.4 GHz multi-angle SMOS observations using 'a priori knowledge' of surface cover fractions. *Proceedings of IGARSS 2004*, *7*, 4552−4555.

Wang, J. R., & Choudhury, B. J. (1981). Remote sensing of soil moisture content over bare field at 1.4 GHz frequency. *Journal of Geophysical Research*, *86*, 5277−5282.

Wigneron, J. -P., Kerr, Y. H., Waldteufel, P., Saleh, K., Escorihuela, M. -J., Richaume, P., Ferrazzoli, P., De Rosnay, P., Gurney, R., Calvet, J. -C., Grant, J. P., Guglielmetti, M., Hornbuckle, B., Mätzler, C., Pellarin, T., & Schwank, M. (2007). L-band microwave emission of the biosphere (L-MEB) model: Description and calibration against experimental data sets over crop fields. *Remote Sensing of Environment*, *107*(4), 639−655.